CHEMICAL ENGINEERING TRANSACTIONS
VOL. 57, 2017
A publication of AIDIC
The Italian Association of Chemical Engineering
Online at www.aidic.it/cet
Guest Editors: Sauro Pierucci, Jiří Jaromír Klemeš, Laura Piazza

ISBN 978-88-95608- 48-8; **ISSN** 2283-9216

Measurement of Gas Hold-up Distribution in Stirred Vessels Equipped with Pitched Blade Turbines by Means of Electrical Resistance Tomography

Antonio Busciglio[a*], Michal Opletal[b], Tomáš Moucha[b], Giuseppina Montante[a], Alessandro Paglianti[c]

[a] Dipartimento di Chimica Industriale "Toso Montanari", Alma Mater Studiorum – Università di Bologna via Terracini 34 40131 Bologna, Italy
[b] Department of Chemical Engineering, University of Chemistry and Technology, Prague Technická 3, 166 28 Praha 6 − Dejvice, Czech Republic
[c] Dipartimento di Ingegneria Civile, Chimica, Ambientale e dei Materiali, Alma Mater Studiorum – Università di Bologna via Terracini 34, 40131 Bologna, Italy
antonio.busciglio@unibo.it

Gas dispersion is a widespread operation in the process industry. The effectiveness of the dispersion affects fluid mixing, heat and mass transfer rates and, as a consequence, the chemical or biochemical reactions involved.
In this work, the gas-liquid dispersion in stirred tanks equipped with pitched blade turbines (PBT) is investigated by means of Electrical Resistance Tomography (ERT). The main goal of this study is the assessment of gas-distribution in the vessel. Measurements are taken in case of different fluid dynamic regimes, which occurrence depends on the operating conditions.
The effect of impeller rotational speed on gas-liquid dispersion is investigated in vessels having different sizes. The adoption of ERT allows the assessment of gas distribution through the vessel volume without any particular limitation about the maximum gas volume fraction, so that experimental conditions close to that adopted in industrial operation can be effectively managed.
The transition between flooding and loading regime is investigated, in which the impeller starts to effectively distribute the gas throughout the liquid phase. The vessel size is found to play a role in determining the condition at which loading regime occurs.
The data could be either used to set up simplified correlations for the transition between flooding/loading regimes or as a valuable benchmark for CFD simulation, given the detailed information available about the spatial distribution the dispersed gas.

1. Introduction

Several chemical reactions involving a gas-liquid or a gas-liquid-solid dispersion are carried out in mechanically agitated tanks (Aubin et *al*., 2004). In general, gas-liquid dispersions are effectively realized using one or more Rushton turbines, or other kinds of radial turbines purposely developed to increase the impeller operability (Nienow, 1998). Mixed flow impellers such as the PBT were found to give rise to fluid flow and torque instabilities in case of down-pumping operation due to the switch between different impeller loading regimes, especially with small gas spargers (Nienow, 1998). On the other hand, mixed-flow turbines allow to effectively disperse a sparged gas phase while suspending solids, so resulting into effective three-phase operations (Frijlink et *al*., 1984; Bujalski et *al*., 1990).
In the "direct loading" regime, the bubbles formed at the gas sparger directly enter the impeller swept volume, and they are dispersed throughout the vessel volume. In the "indirect loading" regime, conversely, the liquid pumped by the impeller drags the bubbles coming from the gas sparger away from the impeller region. The gas phase is firstly recirculated in the vessel volume, and then it reaches the impeller. In general, the critical

impeller speed for direct/indirect loading transition, N_c, depends on the blades angle, the gassing rate Q_g, and the distance between the impeller and the sparger. The N_c value was found to depend on gassing rate according to a power law with exponent equal to 0.5 (Warmoeskerken et *al*., 1984) or 0.4 (Bujalski et *al*., 1988). In Machon et *al*. (1991), a simple model was developed for the transition between indirect/direct loading of down-pumping PBT, based on the assumption that indirect loading starts to occur when the liquid velocity below the impeller exceeds the terminal velocity of bubbles generated at the sparger. In this case the model development led to N_c proportional to $Q_g^{0.2}$.
The regime transitions in case of axial impellers were investigated by means of analysis of the power input curves (Frijlink et *al*., 1984, Machon et *al*., 1991), eventually coupled with rotating video cameras (Warmoeskerken et *al*., 1984), while a quite larger literature exists on the regime transitions in stirred vessels equipped with radial turbines (Middleton and Smith, 2004). Recently, Electrical Resistance Tomography (ERT) was found a viable instrument for the analysis of gas-liquid dispersion regimes (Wang et *al*., 2000; Takriff et *al*. 2013; Lee et *al*., 2014), allowing the non-intrusive characterization of local values of dispersion properties under different operating conditions, including the cases with high overall gas holdup. The potential application of ERT to gas liquid systems includes the measurement of liquid mixing times (Montante and Paglianti, 2015; Patel et *al*., 2013), as well as the bubble concentration distribution in all cases where a conductivity difference exist between the two phases.

2. Experimental set-up and methods

Experiments were carried out in two flat-bottom stirred vessels of different sizes (vessel diameters T equal to 0.232m and 0.480m, hereafter referred to as T23 and T48 respectively), equipped with four baffles (baffle width w equal to T/10). The impeller clearance C was set at 0.5T from the vessel bottom, and a downward-pumping 4-bladed Pitched Blade Turbine (PBT, impeller diameter D equal to 0.4T, blade angle 45°) was used. Water level was always set at H = T. Degassed and demineralized water was used for all experiments. A controlled amount of salt was added (0.1 g/L) to reach a sufficient liquid conductivity for ERT measurements without affecting the density, viscosity and coalescing behaviour of gas bubbles in demineralized water. The gas (air) was injected in the vessels by using circular spargers (diameter D_s, with n_h holes of diameter equal to d_h, details are given in Table 1) placed below the impeller at a distance C_s from the vessel bottom.
Experiments in T23 were conducted at a gassing rate Q_g equal to 15 lpm (1.53vvm) and impeller speeds in the range N = 200-800 rpm, so resulting into fully turbulent regime ($Re = \rho_l D N^2 / \mu_l = 2.93 \cdot 10^4$-$2.93 \cdot 10^5$, $Fr = N^2 D / g$ = 0.1-1.68 and $Fl_g = Q_g / (N D^3)$ = 0.094- 0.023). Experiments in T48 were carried out at impeller speeds in the range in the range N = 140-480 rpm, matching the Fr and Fl_g numbers adopted in T23. This resulted into a gassing rate of 91.5 lpm (1.1vvm).
The electrodes were squared stainless steel plates of side length l_e (see Table 1 for details). Electrodes were arranged in two planes, each containing 16 equally spaced plates. The lower plane, P1, was placed at a distance of 0.24T (in T23) and 0.125T (in T48) below the impeller plane. The upper plane was placed at a distance of 0.19T (in T23) and 0.375T (in T48) above the impeller plane. The electrodes were connected to the data acquisition system (DAS) by coaxial cables.
The conventional circular adjacent strategy was employed for the voltage measurements. The injected current had a frequency of 9.6 KHz and an intensity of 1.5mA. Further details on the ERT method can be found in Montante and Paglianti (2015).
The temperature during the experiment was kept close enough to the reference temperature ($T_{exp} = T_{ref} \pm 0.2$°C) so that the conductivity changes due to temperature could be neglected. In this work, equations to compute the local hold-up value from local mixture conductivity were not used to avoid adding uncertainty and/or subjectivity to the measure data.

Table 1: Dimensions of stirred vessels, gas spargers and electrodes adopted.

	T (mm)	D	C	D_s (mm)	C_s (mm)	d_h (mm)	n_h	l_e (mm)
T23	232	0.4T	0.5T	0.34D	0.384T	0.5	20	20
T48	480	0.4T	0.5T	0.42D	0.27T	2	35	32

3. Results and discussion

The gas liquid dispersion characteristics within the vessel can be inferred from the dimensionless conductivity values σ measured by ERT, i.e. the ratio between the local conductivity in the two-phase conditions divided by the pure liquid conductivity (i.e. the measured reference conductivity). Hence, smaller values of local conductivity are found where larger local gas hold-up is present.

In Fig.1, the distribution of local conductivity is reported in the two planes investigated at two different impeller speeds (N = 200 rpm and N = 650 rpm) at the same gas flowrate, Q_g, of 1.5 vvm. Data measured at N = 200 rpm (Fig.1.a) show the gas distribution with a partially flooded impeller. The gas bubbles generated at the sparger are only hardly dragged to the lower plane, while most of them invade the impeller swept volume and continue their path toward the free surface. However, some bubble breakup occurs at the blade tips. Such smaller bubbles are spread over the upper volume of the vessel. The simultaneous presence of large rising bubbles and smaller bubbles that are dragged by the liquid leads to larger gas content in P2 with respect to P1. In this regime, an increase of impeller speed at fixed gas flow rate has small effect on the gas distribution below the impeller plane, while a gradual spreading of gas phase across the upper vessel volume occurrs. At the critical impeller speed N_c, bubbles start to be dragged away from the impeller before entering the impeller swept volume. Hence, the gas phase invades the lower vessel volume, and only after its recirculation invades the impeller swept volume. The overall gas distribution in case of developed indirect loading regime is shown in Fig.1.b, in which a condition of $N>N_c$ is reported ($N_c \approx 475$, $Fr_c \approx 0.5$, $Fl_{g,c} \approx 0.04$ for T23). The gas clearly appears to be more evenly distributed across the investigated planes, even if some radial gradients of gas hold up are still apparent, especially in P2.

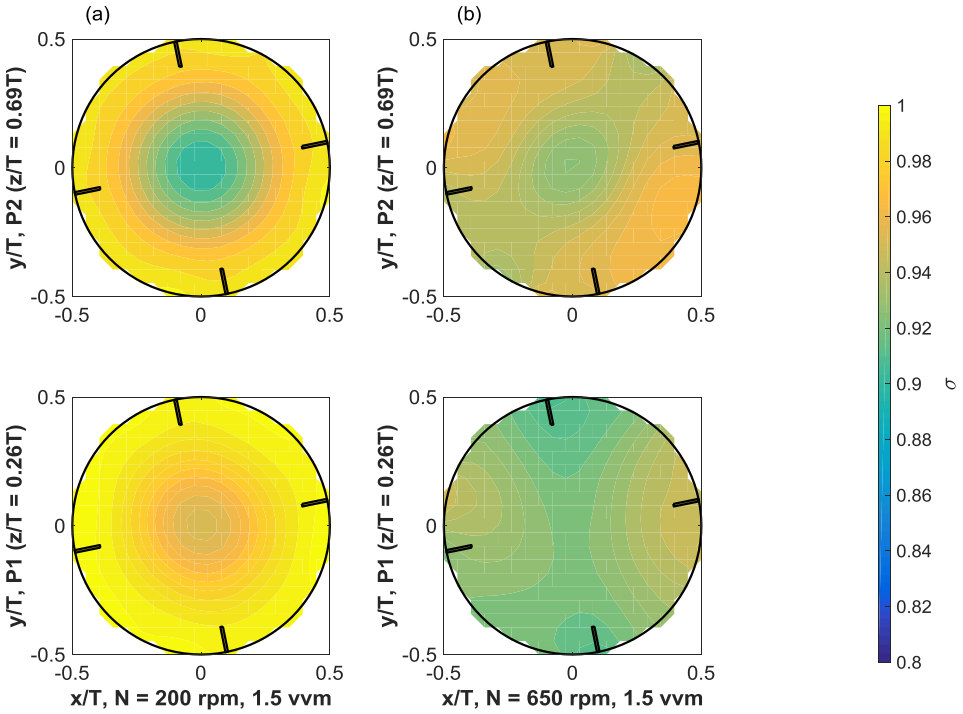

Figure 1: Dimensionless conductivity in T23, at Q_g = 1.5 vvm (a: N= 200 rpm: Fr = 0.105, Fl_g = 0.094; b: N= 650 rpm: Fr = 1.11, Fl_g = 0.029).

The gas distribution can be better discussed from the analysis of the radial profiles of (1-σ), a quantity proportional to the gas phase holdup (Montante and Paglianti, 2015), reported in Fig.2.a-b. The standard deviation of 1- σ values having the same radial coordinates were also computed and reported in Fig.2.a-b as error bars, so giving an indication about azimuthal inhomogeneity of gas dispersion.

At N = 200 rpm, very few gas is dragged toward P1 (Fig.2.a), mainly at the centre of the vessel. The gas content in the P2 is larger, but barely reaches the vessel wall because of the still ineffective impeller action (Fig.2.b). At N = 350 rpm the action of the impeller is more effective, since the gas content in P2 increases. The gas hold-up profile appears to be only translated toward larger values, while its shape is barely affected by impeller speed. The gas phase reaches the vessel wall, but the radial gradient of gas holdup is still apparent. At N = 650 rpm, i.e. after that the indirect/direct loading transition occurred, as expected a quite different distribution of gas phase can be observed. P1 shows a quite larger gas content than that observed at N = 350 rpm, and the gas is more evenly distributed across both planes. Notably, the gas content in the lower plane slightly exceeds the one in the upper plane. This is mainly due to the strong recirculation loop occurring

in the lower half of the vessel (Aubin et *al.*, 2004) that allows the accumulation of the gas phase in the annular region between the impeller and the vessel wall.

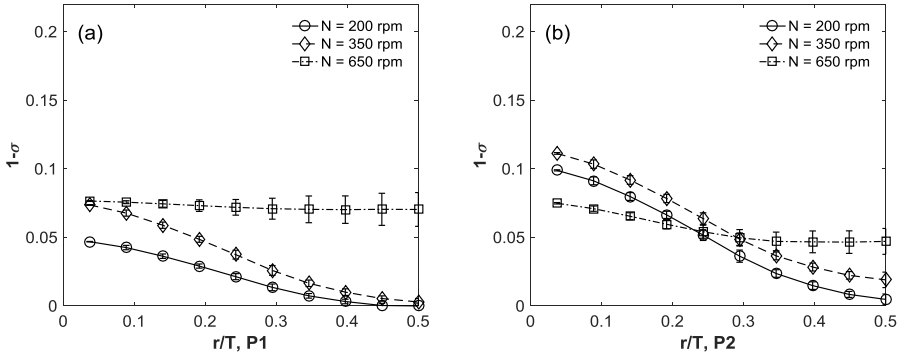

Figure 2: Radial profiles of (1-σ) in T23 at Q_g = 1.5 vvm (a: P1; b: P2).

In the T48 vessel at the same values of dimensionless Fr and Fl_g numbers, similar results are obtained, as it can be seen in Fig.3.

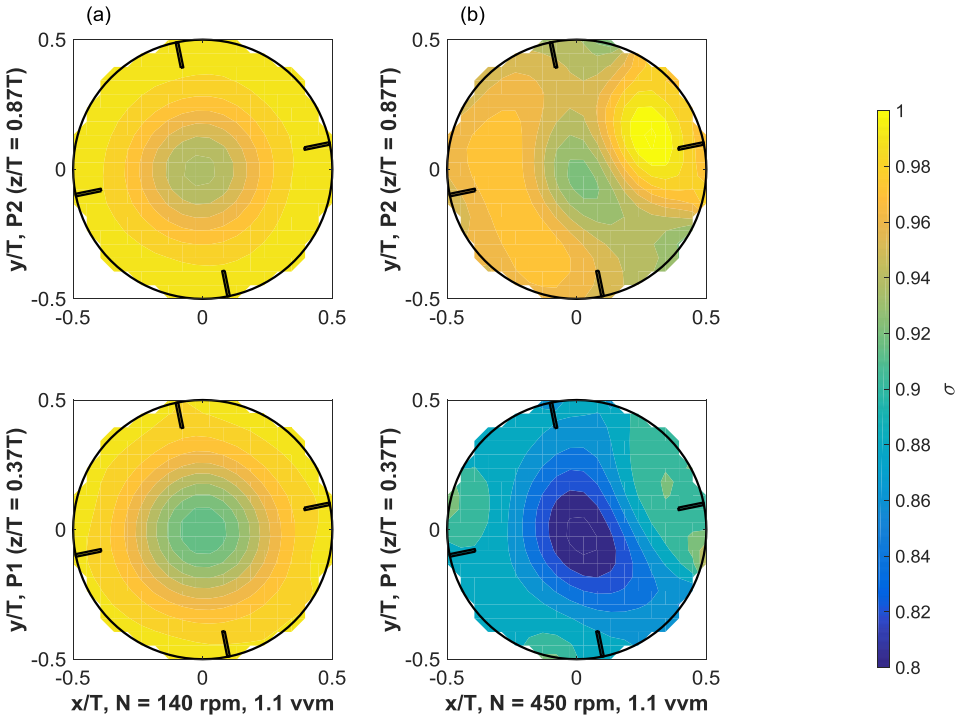

Figure 3: Dimensionless conductivity distribution in T48, at Q_g = 1.1 vvm (a: N= 140 rpm, Fr = 0.106, Fl_g = 0.092; b: N= 450 rpm, Fr = 1.10, Fl_g = 0.029).

The difference between tomograms reported in Fig.1 and Fig.3 is likely due to the different relative position of P1 and sparger. In the T48 vessel, the sparger is placed below P1, hence the high gas hold-up region below the impeller remains visible also in case of indirect loading regime, while in T23 the sparger is placed above P1. Other qualitative aspects of the gas distribution appear to be similar to those observed in the T23 vessel. The radial profiles of (1-σ) for T48 are shown in Fig.4. The radial profiles of 1-σ in T48 (Fig.4) shows that in case of direct loading regime, i.e. at the two lower impeller speeds shown (N_c ≈ 350, Fr_c ≈ 0.65, $Fl_{g,c}$ ≈ 0.037 for T48), the gas phase has a radial distribution similar to that observed in T23 (Fig.2). Conversely, the gas concentration in case of indirect loading regime shows significant radial gradients in T48 (Fig.4) that are not

visible in T23 (Fig.2). The differences observed in the holdup values are likely due to the different vertical position of P1, so intersecting the gas recirculation loops in different positions.

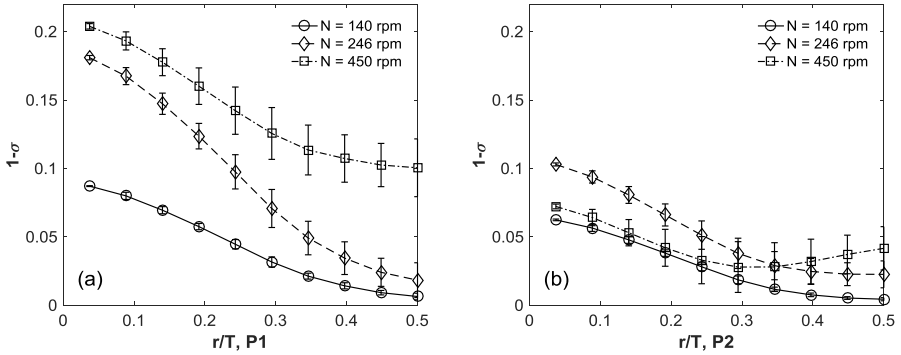

Figure 4: Radial profiles of (1-σ) in T23 at Q_g = 1.1 vvm (a: P1; b: P2).

The overall gas hold-up data in P1 and P2 are reported in Fig.5.a-b respectively. For the T23 vessel, the gas content in P1 has an abrupt change when the direct-indirect regime transition occurs. The same transition cannot be easily seen in T48. Conversely, data collected above the impeller plane show a nice agreement at the two different scales, even if slightly larger gas content is observed in the T23 vessel. The standard deviation of averaged conductivity across the plane (σ_{av}) in repeated data was always smaller than 0.15%, while the standard deviation of local conductivity was smaller than 1% in all cases, so confirming the satisfying data reproducibility, also apparent from Fig.5, where repeated experiments result into practically overlapped points.

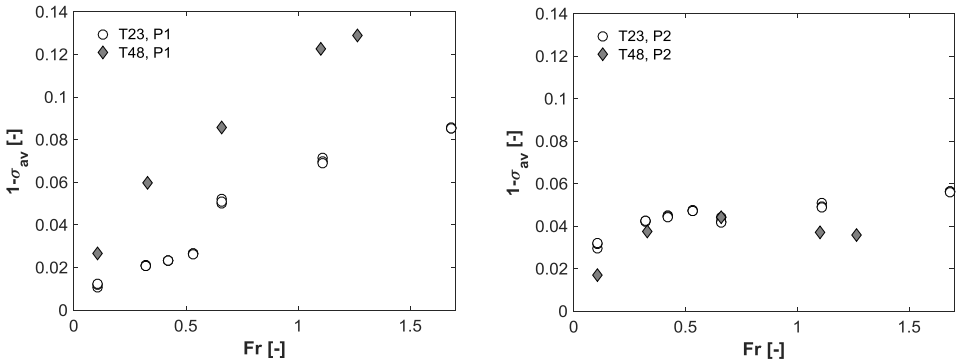

Figure 5: Averaged 1-σ values as a function of Froude number in (a) P1, (b) P2.

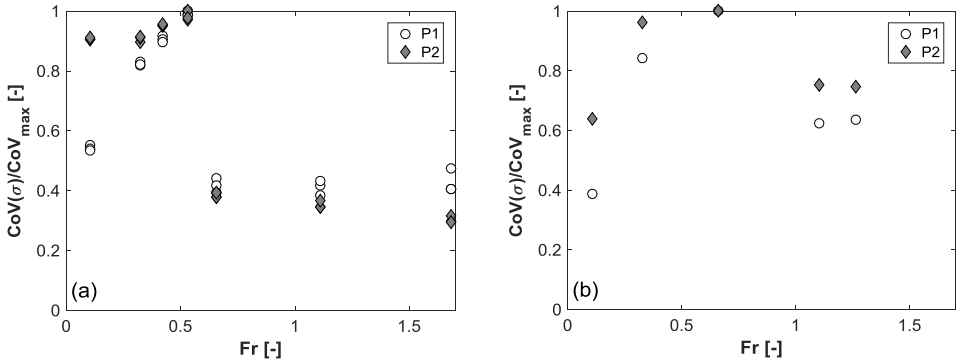

Figure 6. Averaged normalized CoV(σ) values as a function of Froude number for (a) T23, (b) T48.

The analysis of normalized CoV values (computed as the ratio between the CoV and the maximum CoV value measured in that plane) shown in Fig.6.a-b for the T23 and T48 vessel respectively allows to better highlight the conditions at which the transition occurs, i.e. the Fr number at which a discontinuity in the CoV curve occurs.
The CoV data also highlight that significant inhomogeneity of gas distribution is apparent even in P2 under indirect loading regime, and that such inhomogeneity is increased at the larger scale.
On overall, even if the experiments were conducted matching the values of the Fr and Fl_g numbers (see Nienow, 1998; Middleton and Smith, 2004), some differences were found in the gas-phase behavior, and in the conditions at which the indirect/direct loading transition occurred. This is likely due to the bubble terminal velocity, that remains practically constant in the two vessels (for bubble sizes in the range 1-20mm as those observed in the present work, bubble terminal velocity is about 0.2 m/s), while the liquid velocity field is a function of impeller size and speed (proportional to N D). The average bubble size is expected to depend on of gas flowrate, orifice sizes and turbulence levels (Scargiali et *al*., 2014). The T48 vessel, in which larger fluid velocity are generated by the impeller action, is expected to give rise to a more effective gas drag in the main recirculation loop, so resulting into larger gas content in P1. Hence, the need for accurate data on local distribution of gas-phase (as those available from ERT) becomes apparent, especially in case of high values of gas holdup to set up and validate more complex models, since simple dimensional analysis can only partially account for the system complexity.

4. Conclusions

The gas dispersion in a gas-liquid stirred vessel agitated by a down-pumping 4-bladed pitched blade turbine was investigated by means of Electrical Resistance Tomography. Vessels of two different sizes were studied in this work. Experimental conditions were chosen so that experiments in the two vessels were conducted under geometrical and dynamic similarity, i.e. at equal values of the Froude and Gas-Flow number.
The ERT allowed to study in detail the conditions leading to the direct/indirect loading transition, highlighting the differences arising when different vessel scales are considered, without any particular limitation about the gas phase hold-up. The insight into gas-liquid dispersion gained with the adoption of ERT is of great importance for the future development of comprehensive models for such systems.

Reference

Aubin J., Le Sauze N., Bertrand J., Fletcher D.F., Xuereb C., 2004, PIV measurements of flow in aerated tank stirred by a down- and an up-pumping axial flow impeller, Exp. Therm. Fluid Sci., 28, 447-456.

Bujalski W., Konno M., Nienow A.W., 1988, Scaleup of 45° pitch blade agitators for gas dispersion, Proc. of the 6th European Conference on Mixing, Pavia, BHRA Fluid Eng. Centre, Cranfield UK, 389-398.

Bujalski, W., Nienow, A.W., Huoxing, L., 1990. The use of upward pumping 45° pitched blade turbine impellers in three-phase reactors. Chem. Eng. Sci. 45, 415–421.

Frijlink J.J., KolijnM., Smith J.M., 1984, Suspension of solids with aerated pitched blade turbines, Fluid Mixing II, The Inst. of Chem. Eng. Symp. Series, No.89, 49-58

Lee B.W., Dudukovic M.P., 2014, Determination of flow regime and gas hold-up in gas-liquid stirred tanks, Chem. Eng. Sci., 109, 264-275.

Machon V., Fort I., Antosova E., Spanihel B., Kudrna V., 1991, Gas flooding of an inclined blade impeller, Collect. Czech. Chem. Commun., 56, 636-645.

Middleton J.C., Smith J.M, 2004, Gas-liquid mixing in turbulent systems, in Paul E.L., Atiemo-Obeng V.A., Kresta S.M. (Eds.) Handbook of Industrial Mixing, John Wiley & Sons Inc., Hoboken, New Jersey, 585.

Montante G., Paglianti A., 2015, Gas hold-up distribution and mixing time in gas-liquid stirred tanks, Chem. Eng. J., 279, 648-658

Nienow A.W., 1998, Hydrodynamics of stirred bioreactors, Appl. Mech. Rev., 51(1), 3-32.

Patel D., Ein-Mozaffari F., Mehrvar M., 2013, Using tomography technique to characterize the continuous-glow mixing of non-newtonian fluids in stirred vessels, Chem. Eng. Trans., 32, 1465-1470, doi: 10.3303/CET1332245

Scargiali F., Busciglio A., Grisafi F., Brucato A., 2014, Bubble formation at variously inclined nozzles, Chem. Eng. Technol., 37(9), 1-9.

Takriff M.S., Ahmad A., Rosli M.I., Jantan S., 2013, ERT visualization of gas dispersion performance of aerofoil and radial impellers in an agitated vessel, Journal Teknologi, 64:5, 75-78.

Wang M., Dorward A., Vlaev D., Mann R., 2000, Measurements of gas-liquid mixing in a stirred vessel using electrical resistance tomography (ERT), Chem. Eng. J., 77, 93-98.

Warmoeskerken M.M.C.G., Speur J., Smith J.M., 1984, Gas Liquid dispersion with pitched blades turbines, Chem Eng Comm., 25, 11-29.